流下液膜に生ずる馬蹄形表面波（渦）の運動特性

Evolution of solitary waves and nearly sinusoidal waves on a vertically falling liquid film

Nosoko, T., Miyara, A. and Nagata, T.

Department of Mechanical and Systems Engineering, University of the Ryukyus, Nishihara, Okinawa 903-0213, Japan

1. Introduction

Liquid films falling down a vertical or inclined surface show a hydrodynamic instability which causes surface waves evolving on the films. The earliest theoretical studies into the hydrodynamic instability started with the linear stability analysis based on the Orr-Sommerfeld equation. The Orr-Sommerfeld equation is derived from the Navier-Stokes equations and the continuity equation by introducing the two-dimensional disturbance η represented by

$$\eta = \delta \exp\{i(\alpha x - \omega t)\} \tag{1}$$

where δ, ω ($=2\pi f h_o/u_o$, h_o: Nusselt film thickness, u_o: average velocity, f: wave frequency) and α ($=2\pi h_o/\lambda$, λ: wavelength) are the initial amplitude, the dimensionless angular frequency and the dimensionless wave number. When α is allowed to be complex, sinusoidal waves with an amplitude δ at the film inlet exponentially grow or decay 'spatially' in the direction of film flow. When ω is complex, the film is initially covered with sinusoidal waves with amplitude δ, which exponentially grow or decay with time or 'temporally'. Benjamin (1957) and Yih (1963) found approximate analytical solutions to the temporal Orr-Sommerfeld equation for the cases of low Reynolds number or very low wave number α. Then, approximate solutions not restricted to small Reynolds number were developed by

Anshus and Goren (1966) and Krantz & Goren (1971). Krantz & Owen (1973) showed that the approximate solutions to the spatial Orr-Sommerfeld equation are in much better agreement with experimentally measurements of wave growth rates for falling films of low surface tension on a vertical surface. Whitaker (1964) and Pierson and Whitaker (1977) numerically solved the Orr-Sommerfeld equation without any assumption for a water film falling down a vertical surface at Reynolds numbers Re = 10/3, 20/3, 100/3, 200/3, 1000/3 and 2000/3, and found that the solutions to the spatial and temporal equations are in good agreement with each other except at Re = 100/3 and 200/3 where discrepancies occur in the wave number α_m corresponding to the maximum growth rate by % and %, respectively. These linear stability analyses for falling films on a vertical surface showed that wave growth rate begin at the origin, rapidly increases with wave number to the maximum and then monotonously decreases, and that the dimensionless wave velocity $c_r = c/u_o$ is 3 at vanishing wave number, rapidly decreasing with wave number to the minimum, and then monotonously increases. The monotonously decreasing growth rate curve intersects the axes of zero growth rate where the disturbances are 'neutral', i.e. they neither grow nor decay.

The comparison between the solutions to the Orr-Sommerfeld equation and the experimental results (Anshus and Goren (1966), Krantz and Owen (1973) and Pierson and Whitaker (1977)) demonstrated that the solutions of the wave number and the phase velocity of the fastest growing waves roughly predict the experimental measurements of wave number and wave velocity of waves at the inception line with a several centimeter distance from the film inlet (Kapitza and Kapitza (1949), Stainthorp and Allen (1965), Jones and Whitaker (1966), Strobel and Whitaker (1969), Tailby and Potalski (1962) and Pierson and Whitaker (1977)). These waves

originated from the ambient noise and 'naturally' occurred on falling films on vertical surfaces without any attempt to impose disturbances on the films.

Visible real waves on the films are not linear or not sinusoidal, but are nonlinear. Approximate nonlinear stability theories have been developed to study the wave evolution subsequent to the wave inception. Benny (1966) derived a single nonlinear evolution equation for the film thickness from the Navier-Stokes equations and the continuity equation by assuming small wave number (or long wave, i.e. $h_o/\lambda \cdot 1$) and low Reynolds number at which inertia is small. Lin (1969), Gjevik (1970) and Nakaya (1975) derived the analytical solutions to the long-wave evolution equation and Pumir, Manneville and Pomeau (1983) and Joo, Davis and Bankoff (1991) obtained the complete numerical solution to the extended Benney type equation. They all predicted finite-amplitude steady-traveling waves for wave numbers slightly larger than the neutral wave number α_c. Most of the predicted long waves have longer and flatter valleys between shorter and steeper crests at Reynolds numbers of several units (Lin (1970)). Recently Ooshida (1999) further developed the long-wave evolution equation by combining the Pade' approximation with the long-wave expansion, and showed that his solutions to the developed equation are in agreement with the experimental results of steady traveling wave profile on a vertical ethanol film at Re = 9.1 by Kapitza and evolving wave profiles on a slightly inclined glycerin-water solution films of $\beta = 4.6$ at Re = 23 by Liu et al.

Alekseenko et al. (1985) derived coupled integral boundary layer equations for film thickness and local flow rate by introducing a parabolic velocity profile in the film and boundary layer assumption. Bunov, Demekhin and Shkadov (1984) assumed steady- traveling waves and solved the integral boundary layer equations. They found that there exist two families of waves, i.e. the first family has phase velocities smaller

than $3u_o$ and transform wave profile with an decrease in wave number from the neutral wave number α_c from sinusoidal waves via double-peaked ones into the negative solitary humps (steep and deep valleys), and the second family has phase velocities larger than $3u_o$ and transform the profile from sinusoidal waves via tear-drop waves with a single front-running small wave into positive solitary humps with front-running small waves. The profiles of the double-peaked waves and the negative solitary humps of the first family are the same as these of the tear-drop waves with a single front-running wave and the solitary humps, respectively when the former profiles are turned upside down. The solutions by Demekhin, Tokarev, Shkadov (1987) and Tsvelodub (1990) are in good agreement with the experimental measurements of wave profiles on films falling down vertical walls at Re = 8.0 and 7.5 by Alekseenko, et al. (1985) and Nakoryakov, Pokusaev and Alekseenko (1983).

The boundary layer equations without introduction of any velocity profile in the film are derived by omitting the second derivative $\partial^2/\partial x^2$ term in the Navier-Stokes equations and introducing the long-wave approximation $\partial/\partial y \gg \partial/\partial x$, and first studied by Shkadov et al (1970). Chang, Demekhin and Kopelevich (1993) numerically solved the steady-traveling two-dimensional boundary layer equations and found the two wave families which have basically the same characteristics as those found by Bunov, Demekhin and Shkadov (1984). Their numerical solutions are in good agreement with the experimental measurements of wave profiles on falling water films on vertical walls obtained at Re < 31 by Kapitza and Kapitza (1949), Nakoryakov et al. (1985) and Stainthorp and Allen (1965). Chang et al also performed stability analyses of these waves and indicate that all waves are unstable to three-dimensional disturbances with small growth rate. Chang, Demekhin and Kalaidin (1996) numerically solved the transient boundary layer equations with the

boundary condition of imposing very small amplitude disturbances of various frequencies with random phases at the inlet of computation domains of 2.5 m or less lengths in the flow direction for a water film falling down a vertical wall at Re ~ 8 or less, and demonstrated that the solutions are in good agreement with the experimental measurements of the variation of wave velocity in downstream direction at Re ≤ 45 and the variation of distance between the film inlet and the wave inception line with Reynolds number at Re ≤ 80. Their detail examination of the solution for a 2.5 m long film at Re = 18.75 showed that the film surface is nearly smooth in a distance from the entrance, where the disturbances of frequency f ~ f_m exponentially grow, and then the disturbances rapidly develop into visible sinusoidal waves, closely packed tear-drop shaped humps and then solitary humps with front-running capillary waves in approximately 10 wavelength distance. These solitary humps coalesce several times with neighbors at different distances to change into saturated stationary humps with larger velocities and larger separations. After wave inception, the average wave velocity decreases to the minimum as nearly sinusoidal waves grow into tear-drop waves and then gradually increase downstream to the saturated velocity at x ~ 1.2 m or larger. This gradual increase in the wave velocity is caused by coalescence of neighboring humps to form a single rump of larger peak.

Direct numerical studies of the complete Navier-Stokes equations have also been performed by Bach and Villadsen (1984), Kheshgi and Scriven (1987), and Malamataris and Papanastasiou (1991), and by Ho and Patera (1990), Nagasaki and Hijikata (19), Salamon, Armstrong and Brown (1994) and Ramaswamy, Chippada and Joo (1996) using the finite elemnt method and alternative methods, respectively to handle the moving boundary, i.e. the film surface. Salamon et al. (1994) solved the steady-state Navier-Stokes equations with the assumption of the existence of steady

traveling waves, and Nagasaki and Higikata (199) solved the transient Navier-Stokes equations coupled with the periodic boundary conditions, i.e. the film thickness and flow conditions at the film inlet are the same as those at the exit of the computation domain. The solutions obtained with the periodic conditions predict 'temporal growth' of waves which may approximately be converted to the wave growth in the flow direction ('spatial growth') by assuming the wave propagation distance equal to the integration of the wave velocity with respect to time. The spatial wave growth is directly predicted with the non-periodic boundary conditions. Ramaswamy, Chippada and Joo (1996) employed the non-periodic boundary conditions, as well as the periodic boundary conditions with very long computation domains. These three research groups used mesh points on the spines vertically stretching from the wall to the film surface, and the mesh points slide up and down along the spine depending on local film thicknesses varying with time. Ho and Patera (1990), Salanom et al. (1994) and Ramaswamy et al. (1996) obtained fairly good agreement with the experimental results of Kapitza and Kapitza (1949) and the solutions to the integral boundary layer equations for profiles of solitary tear-drop waves and closely packed waves at Re = 6 and 20, respectively on a vertically falling film. Nagasaki and Hijikata (199) numerically constructed steady traveling waves, i.e. nearly sinusoidal waves, closely packed tear-drop waves and solitary tear-drop humps with front-running capillary waves, at Re = - by decreasing wave number. Their results for wave velocity and peak height are fitted by the empirical correlation by Nosoko et al (1996). Most results of Ramaswamy et al. (1996) with the non-periodic boundary conditions were obtained for a falling film on slightly inclined plane (inclination angle from a horizontal plane, β = 6.4°) at Re = 179, which is imposed disturbances of a single frequency at film inlet. They numerically constructed spatial growth of the

disturbances into nearly sinusoidal saturated waves with gentle wave peaks and sharp valleys, closely packed quasi-periodic tear-drop waves with a front-running single capillary wave and saturated solitary tear-drop humps with capillary waves by decreasing the frequency of disturbances. The disturbances at an intermediate frequency develop into the closely packed tear-drop waves with a single capillary wave via transient double-peaked waves, i.e. two peaks forming a small depression between them on a hump. They found very good agreement with the experimental results of Liu and Gollub (1994) for the wave growth at different frequencies, the saturated wave profiles, and the quasi-periodic behavior of the closely packed tear-drop waves.

It is very difficult to experimentally produce two-dimensional waves on a film falling down a vertical wall since the waves are unstable to three-dimensional noise and very slight imperfection of a film inlet manifold imposes three-dimensional noise on the film flow. When two-dimensional and three-dimensional noise are diminished as small as possible, wave appear at a distance from the film inlet, and then soon develop into three-dimensional waves. These naturally occurring (or noise-driven) waves have extensively been examined in numerous experiments by Stainthorp and Allen (1965), and Portalski and Cleyg (1972), Pierson and Whitaker (1977) to determine the distance from inlet to the wave inception line, wave velocity and wave number at the wave inception line. Stainthorp and Allen (1956) measured the variation of wave velocity in the downstream direction and wave profiles by detecting intensity of a light beam passing through a dyed film.

Waves keep two-dimensionality in longer distances when imposing two-dimensional disturbances of a single frequency on the film flow at the inlet. The two-dimensional waves forced to occur at the same frequency as the disturbances

have also been studied for vertically falling films by Kapitza and Kapitza (1949), Krantz and Goren (1971), Alekseenko et al. (1985) and Nosoko et al. (1996) and for slightly inclined films by Liu et al (1993) and Liu and Gollub (1993, 1994). Kapitza and Kapitza (1949) and Alekseenko et al. (1985) captured the profiles of steady traveling waves at various frequencies at Re = - . Krantz and Goren (1971) determined the wave velocity and the growth rate of exponentially growing waves as functions of wave number at Re ~ 1 or less. Nosoko et al. (1996) determined wave velocity of steady traveling waves as a function of wave number and Re or of wave peak height at Re = - . Liu et al. (1993) and Liu and Gollub (1993, 1994) captured the profiles of growing, steady traveling or quasi-periodic waves of films on slightly inclined plane.

Recently Miyara (2002) developed the direct numerical simulation which is applicable to two-dimensional flow of vertically falling films at larger Reynolds numbers. Nosoko et al. (1996) achieved two-dimensional waves in larger distances on a vertically falling film at larger Reynolds numbers, and observed the waves by means of shadowgraph. In the present work, we experimentally and numerically explored evolution of two-dimensional waves on a water film falling down a vertical surface when imposing two-dimensional disturbances of a single frequency on the water film at the inlet.

2. Experimental apparatus and procedure

A cross-section or the test section is shown in Figs. 1 and 2, which consists of a rectangular frame and a glass plate. Tap water from a head tank flows through a silicone tube into the holding compartment where the water is distributed transversely. The water passes through a 0.5 mm gap between the glass plate and the bar with a

sharp edge, and then forms a film falling down the vertical glass plate. The film flow rate is perturbed at a constant frequency f with small amplitude by periodically pressing the silicone tube with a thin plate which is derived by a speaker.

Light rays from a stroboscope deflect at the wavy surface of the film to form shadows of waves on the screen. The shadows on the screen are captured by a still camera synchronized with the stroboscope.

3. Numerical method

We performed direct numerical studies of the complete Navier-Stokes equations. Please refer the following paper for the details.

Miyara, A., Nosoko, T. and Nagata, T., Enhancement of heat and mass transfer by waves on falling liquid film, Proceedings of 12th International Heat Transfer, Aug. 18-23, 2002, Grenoble France, in press

4. Results and Discussion

4.1. Overviews on the dynamics of evolving waves

Figures 3 and 5 show numerical constructions of two-dimensional wave profiles for various forcing frequencies at Reynolds numbers of Re = 16.1 and 51.5, and figures 4 and 6 do shadows of surface waves on the screen at the same frequencies and Reynolds numbers. The numerical simulations always include the two-dimensional noise arising from rounding numbers in computer calculations, which may be much smaller than the real ambient noise. In addition, the real noise is not two-dimensional, but three-dimensional. Therefore, the numerical simulations construct the two-dimensional waves occurring only when the ambient noise is two-dimensional and minimized. When disturbances at low forcing frequencies are

put into the numerically constructed film flow at the entrance, small waves appear from the entrance, and then rapidly increase in their peak height to form steep fronts and long gently sloping tails (often referred to as 'tear-drop shape') as the waves travel downwards (the wave profiles of f = 14.0 Hz at Re = 16.1 and f = 25.0 Hz at Re = 51.5 in Figs. 3 and 5). As the fronts become steeper, small 'bow' waves with much smaller wavelengths than those of the primary waves are generated immediately downstream and increase the number of themselves. The growth of waves saturates in 3 or 4 wavelengths from the entrance, and then the saturated waves travels downwords at almost constant phase velocities in near synchrony. The primary waves are also often referred to as 'solitary humps' (e.g. by H. C. Chang, 1994) because of nonstationary interaction among them. The front-running bow waves are often referred to as 'capillary waves' or 'capillary ripples' (e.g. by Alekseenko, et al., 1985) since their wavelengths are smaller than the capillary constant and strongly depend on the surface tension. As shown by Nosoko, et al. (1996), a solitary hump with higher peak and larger velocity has more number of the front-running bow ripples. When the frequency is increased, the solitary humps are closer together and front-running capillary ripples ride on the tails of the preceding humps (the wave profiles at f = 25.0 Hz and Re = 51.5).

As the forcing frequency is increased further, the waves show an interesting transition behavior (the waves of f = 22.5 Hz at Re = 16.1, and f = 35.1 Hz and 40.1 Hz at Re = 51.5). The waves quickly grow into 'single-peaked waves' with a steep front and a gently sloping tail in 3 wavelengths from the entrance, and then a new small peak appears on the tail of a primary wave and grows to form a 'double-peaked waves' consisting of the newly occurring peak and the old peak. The new peak continuously grows as the old peak decays to disappear, resulting in transformation

into a single-peaked wave. Then a small peak again appears on the tail of the single-peaked waves. This event could happen once to three times in different distances from the entrance, and the number of the events mainly depends on the Reynolds number. In the last event, the decaying peak does not disappear, but forms a steady single capillary ripple. After that, the tear-drop wave with a single capillary ripple travels downstream in quasi-stationary state, i.e. they slightly change their shapes near-periodically. Because of this transition behavior, the quasi-stationary state is established in much larger distances from the entrance than the solitary humps with several capillary ripples and the nearly sinusoidal waves mentioned below.

As the forcing frequency is increased much further, the transition behavior vanishes and tear-drop waves with a gentle peak and a narrow trough per period evolve (the wave profiles of f = 30.0 Hz at Re = 16.1 and f = 46.7 Hz at Re = 51.5), and then travel downstream in quasi-stationary state. The shape of waves becomes nearly sinusoidal with increasing frequency, associating with a decrease in the growth rate (the wave profiles of f = 100.2 Hz at Re = 51.5).

When the forcing frequencies larger than the neutral frequency, sinusoidal waves of a small wavelength gradually decay to disappear, and then new waves with much larger wavelengths rapidly grow into solitary waves (the wave profile of f = 85.3 Hz at Re = 16.1 in Fig. 3).

The numerically constructed film surface is always smooth when the periodic disturbances are not put into the film flow. This may be because the numerical noise arising from rounding numbers is too small to develop into visible waves within the numerically observed film length.

With the present optical set up each solitary hump with front-running capillary waves and each single-peaked wave produce a train of dark and light stripes and a pair

of a dark strip and a light one on the screen, respectively as shown in Figs. 4 and 6 since the concave surfaces and convex ones of the film cause the light rays from the stroboscope to diverge and converge. Deep troughs of waves cause darker stripes, and therefore the deepest trough just in front of the solitary wave forms the darkest strip in the train (the shadows of f = 14.0 Hz at Re = 16.1 and f = 25.0 Hz at Re = 51.5 in Figs. 4 and 6). The real ambient noise in the laboratory may be much larger than the numerical noise and include three-dimensional components. When the periodic disturbances are not applied to the experimental film flow, the film shows smooth surface in a distance from the entrance, and then single-peaked waves originating from the ambient noise grow (the shadows of f = 0 at Re = 16.1 and Re = 51.5). The length of the smooth surface and the frequency of the single-peaked waves at wave inception are very sensitive to the noise, and therefore both of them vary with time to an extent, resulting in that the single-peaked waves occur with different wavelengths and then velocities and coalesce with a neighbor after traveling several wavelengths to transform themselves into solitary waves with capillary ripples. The length of the smooth surface monotonically increases with Re in the present experimental range of Re when the ambient noise is suppressed as small as possible. According to the experimental data obtained by Stainthorp and Allen (1953) and Tailby and Portalski (1962), the smooth surface length decrease to the minimum at Re ~ 20 and the monotonically increases with Re in the laminar flow range of Re < 400.

The experimentally generated periodic disturbances are primarily two-dimensional and include slightly three-dimensional or transverse components. When the experimental disturbances at low frequency are applied, the periodic disturbances rapidly develop into two-dimensional solitary waves (trains of horizontal dark and light stripes at f = 14.0 Hz in fig. 4 and at f = 25.0 Hz in fig. 6) in two wavelengths

from the entrance, and then the solitary waves gradually develop transverse disturbances due to the three-dimensional instability, resulting in deformed wavefronts (the deformed stripes on the screen). The inception of the transverse disturbances does not fluctuate in space and time, and this was observed at various forcing frequencies and Reynolds numbers (the shadows of f = 14.0 Hz at Re = 16.1 and f = 25.0 – 46.7 Hz at Re = 51.5). Therefore, it is evident that the transverse disturbances originate from imperfection of the entrance manifold.

At intermediate forcing frequencies, evolving waves show the transition behavior, and then develop into solitary waves with a single capillary wave (the shadows of f = 22.5 Hz at Re = 16.1 and f = 40.1 Hz at Re = 51.5). The resultant solitary waves soon interact with the neighbor(s) to develop transverse disturbances of spanwise wavelengths which are approximately same as the streamwise wavelength (the distance between the solitary waves) but much smaller than those of the transverse disturbances originating from the imperfection of the entrance manifold. The former are superimposed on the latter. Then, pairs of the three-dimensional waves coalesce with each other to transform themselves into irregularly deformed three-dimensional waves with larger streamwise wavelengths.

As the forcing frequency is increased further, the transition behavior disappear but the two-dimensional single-peaked waves grow, saturate and then coalesce with neighbor(s) to chang into two-dimensional solitary humps of larger wavelengths associating with front-running capillary ripples (the shadows of f = 30.0 and 32.5 Hz at Re = 16.1). It is observed that two single-peaked waves coalesce at once to change into a solitary hump with capillary ripples at f= 30.0 Hz and Re = 16.1, and three single-peaked waves do into a solitary hump with capillary ripples at f = 32.5 Hz. It is very sensitive to the ambient noise and two, three or more single-peaked waves

coalesce at once. The distance from the entrance at which the wave coalesce also very sensitive to the ambient noise, and the distance of coalescence in general decreases with the increasing forcing frequency when the ambient noise is suppressed as small as possible. The coalescence of waves occurs at larger distances from the entrance at Re = 51.5 (not seen in the shadows of low and intermediate forcing frequencies at Re = 51.5), and the distance of coalescence also decreases with increasing forcing frequency. The numerically constructed waves do not coalesce with each other within the numerically observed film length at Re = 16.1 since the numerical noise is much smaller than the real ambient noise.

When Re is large and the forcing frequency is close to the neutral frequency, the two-dimensional single-peaked waves gradually grow and then transverse disturbances start growing before the two-dimensional waves saturate (shadows of f = 100.2 Hz at Re = 51.5). The resultant deformed waves have isolated depressions, and then are disintegrating associating with a decrease in the wave amplitude to form a rough film surface.

When the forcing frequency is larger than the neutral frequency, the waves gradually decay to disappear, and then new waves with wavelengths much larger than that of the decaying waves rapidly develop into solitary humps with front-running capillary wave(s) (shadows of f = 85.3 Hz at Re = 16.1). The solitary humps have slightly larger wavelengths than the naturally occurring waves. These new humps appear at distances from the entrance much smaller than the numerically constructed waves. This is also due to the real ambient noise much larger than the numerical noise.

In general, the experimental waves show the same dynamic characteristics as the numerical waves, i.e. the evolution of solitary humps with capillary ripples at low forcing frequencies, the occurrence of double-peaked humps in the transition from

single-peaked waves to humps with a single capillary ripple at intermediate forcing frequencies, the evolution of nearly sinusoidal waves at forcing frequencies close to the neutral frequency, and the occurrence of new waves after the decaying of sinusoidal waves at forcing frequencies larger than the neutral frequency. Some differences are observed, i.e. the growth of the transverse disturbances on the solitary humps, the tear-drop waves with a single capillary ripple and the single-peaked waves, and the coalescence of waves are only observed for the real liquid films, and the wave-inception distances from the entrance are much shorter for the real films than the numerical films when the disturbances are not applied. These differences are all due to the real ambient noise with larger amplitudes than the numerical ones, and the periodic disturbances including there-dimensional components.

4.2. Acceleration and Deceleration of Evolving Waves

Figures 7 (a) and (b) shows the experimentally determined variations of wavelength λ with distance from the film inlet for various forcing frequency at Re = 51.5. The wave velocity approximately is equal to a multiple of λ and the forcing frequency, i.e. $u = \lambda f$ when the wave velocity does not changes rapidly, and therefore figure 7 roughly shows the variations of wave velocity u. When the forcing frequency f is low, waves rapidly accelerate within two wavelengths from the entrance, and then the wave velocity reaches a gentle maximum (f = 15.1 and 25.0 Hz in Fig. 7 (a)). After that, the wave velocity gradually decreases as the transverse disturbances grow on the waves (the shadows at f = 25.0 Hz in Fig. 7). These indicate that the two-dimensional disturbances grow much more rapidly than the three-dimensional disturbances when the forcing frequency and wave number are low and that the saturated two-dimensional waves have larger velocity than the three-dimensional

waves.

At intermediate forcing frequencies, the waves show the transition behavior in x = 0 - 100 mm (f = 37.5 and 43.1 Hz in Fig. 7 (a) and (b)), i.e. the waves experience three times the transition from single-peaked waveform to double-peaked wave and vice versa in the transition region x = 0 - 100 mm, and have the minima in wavelength when the waves take single-peaked waveform. The waves have double-peaked waveform between the minima, and then change into tear-drop waves with a single capillary ripple (the numerical profiles of 40.1 Hz at Re = 51.5) just after the last minimum. The resultant tear-drop waves with a single ripple have nearly constant wavelengths and larger velocities than the double-peaked waves.

At large forcing frequencies, waves gradually decrease in velocity (f = 67.1 Hz and 100.2 Hz in Figs. 7 (a) and (b)), and then the measurements of wavelength become scattered as the waves grow the transverse disturbances. As clearly seen at f = 100.2 Hz, the wave velocity does not saturate before the transverse disturbances become intense (f = 100.2 Hz in Figs. 7 (b) and 6).

We determined the velocities of saturated waves using the relation $u = \lambda f$ by taking λ as the average of the maximum wavelengths, the wavelengths of tear-drop waves with a single ripple and the minimum wavelengths just before the scattering of measurements at the low, intermediate and high forcing frequencies, respectively. The average wave velocities were also determined by taking λ as the average over the transition region. These measurements of velocity are shown in Fig. 7. The plate being vibrated by the speaker produces pulse-like disturbances, and therefore the velocity of small-amplitude sinusoidal waves evolving exponentially could not determined at low and intermediate frequencies in the present experiments. When the forcing frequency is near the neutral frequency or larger, it produces nearly sinusoidal disturbances.

We solved the Orr-Sommerfeld equation by means of the approximate solution method developed by Anshus and Goren (1966). Table 1 shows comparison between approximate solutions and the numerical solutions by Pierson and Whitaker (1977) to the Orr-Sommerfeld equation for spatially growing waves. There are excellent agreements in phase velocity c_m for the fastest growing wave, but discrepancies by 8–10% are observed in the wave number α_m for the fastest growing wave and in the critical wave number α_c when Reynolds number is small (Re = 10/3 and 20/3). Discrepancies are very small when Reynolds number is in the range of the present work (Re = 100/3 and 200/3), and therefore we can conclude that the approximate solution method raises small errors in the present range of Reynolds number (Re = 15 – 60).

Figures 8 (a) and (b) show the nondimensional velocities of the exponentially growing sinusoidal waves and of the saturated quasi-stationary two-dimensional waves at Re = 16.1 and 51.5. In this paper we term the phase velocity of the exponentially growing small waves 'the linear velocity' and the one of the saturated quasi-stationary waves 'the nonlinear velocity' after Liu and Gollub (1994). The solid line represents the approximate solution to the Orr-Sommerfeld equation, and the dashed curve is the empirical correlation for solitary humps with capillary ripples by Nosoko et al. (1996). The linear and nonlinear velocities were determined at the same forcing frequencies by the present numerical simulations, and the nonlinear velocity was experimentally measured at various forcing frequencies by means of the method described above.

The nondimensional linear velocity is 3 at the vanishing wave number, α, and it decreases to the minimum and then increases with increasing α. The linear velocity rapidly increases after the minimum at Re = 16.1 while it gradually increases at Re =

51.5. The wave number α_m for the fastest growing sinusoidal waves is near and smaller than the wave number for the minimum linear velocity, and the neutral linear velocity is smaller than 3 at both Re = 16.1 and 51.5. The nondimensional minimum and neutral velocities are larger at Re = 16.1 than Re = 51.5, and the wave number for the minimum velocity and the neutral wave number are smaller at Re = 16.1.

The numerical simulation data for linear velocity are in good agreement with the solutions to Orr-Sommerfeld equation for the various wave numbers at both Re = 16.1 and 51.5. The numerically determined nonlinear velocities are in good agreement with the experimental measurements at both Reynolds numbers for various wave numbers, except for wave numbers near and smaller than the neutral wave number, where the experimentally excited two-dimensional waves start developing the transverse disturbances before the two-dimensional waves reach saturation. Therefore the experimentally determined nonlinear velocity is larger than the velocity of the saturated two-dimensional waves near the neutral wave number since the evolving waves decelerate.

The arrows from plots for linear velocity to plots for nonlinear velocity show that numerical sinusoidal waves excited at the entrance accelerate or decelerate as the waves grow to saturate, keeping the same frequencies as shown in figs. 3 and 5. Nosoko et al's correlation excellently fits the numerical and experimental nonlinear velocity data, and is larger than the linear velocity curve at both Reynolds numbers when the wave number is small. Nosoko et al's correlation intersects the linear velocity curve, showing that evolving waves accelerate when the wave number is smaller than the intersection. The acceleration is larger at smaller wave number (or larger forcing frequency). The wave number of the intersection is slightly smaller than the wave number α_m for the fastest growing waves.

The numerical and experimental nonlinear velocity begins to deviate from Nosoko et al's correlation as the wave number α increases from the intersection, and then reaches the minimum where the nonlinear velocity is smaller and the wave number is larger than the linear velocity and the corresponding wave number. After the minimum, the nonlinear velocity increases more rapidly than the linear velocity, and they merge at the neutral wave number. It is seen that the experimentally determined nonlinear velocity merge with the linear velocity before the neutral point at Re = 16.1 since the excited waves start to coalesce with the neighbors before they saturate. When the wave number is larger than the neutral wave number, the waves excited at the entrance gradually decay to disappear. The numerically and experimentally determined velocities of the decaying waves are in good agreement with the linear velocities.

The transition from the double-peaked humps to tear-drop wave with a single capillary ripple occurs between the intersection of the linear and nonlinear velocity curves and the minimum point of the nonlinear velocity at both Reynolds numbers. The velocity of the double-peaked waves is smaller than the linear velocity, and the velocity of the saturated tear-drop waves with a single capillary ripple is larger than the velocity of the double-peaked waves, showing that the sinusoidal waves with a small amplitude decelerate as they grow into the transient double-peaked waves, and then rapidly grow into the tear-drop waves with a single ripple with a larger velocity.

When the wave number is equal to the one for the minimum nonlinear velocity or larger, the excited waves with a small amplitude monotonously decelerate as the grow into the saturated waves with a single peak per period. The deceleration is largest at the forcing frequency for the minimum nonlinear velocity, and decreases with an increase in wave number. When the wave number is equal to the neutral one or larger,

the excited waves are neutral, i.e. neither grow nor decay, or decaying to disappear. Therefore neither acceleration nor deceleration of waves occur.

4.3. Transition from single-peaked waves to tear-drop waves with a single capillary ripple

Figure 9 shows the time variation of numerically constructed wave profiles of f = 40.1 Hz at Re = 51.5, demonstrating the transition behavior in detail. A small peak newly appears on the tail of a single-peaked wave to form a small depression between the small peak and the primary peak at $x/\delta \sim 340$. The depression moves toward the primary peak and passes it as the newly occurring peak grows and the primary peak decays, showing that the depression travels downstream faster than the primary peak. This event occurs three times, i.e. the first one begins at $x/\delta \sim 120$ and the second one does at $x/\delta \sim 220$. The depression is not clearly observed in the first event, but it is emphasized in the second one and more emphasized in the third and last one. The clearly observed depression passes the primary wave in the last event, and then stays immediately downstream to form a steady single capillary ripple. During the course of the events, double-peaked waves are only temporally observed. Therefore it is evident that they are unstable.

The almost same transition behavior and double-peaked waves were observed on a slightly inclined film of aqueous solution of glycerin by Liu and Gollub (1994). The event occurred only once and much more slowly on their inclined film. The inclination angle from a horizontal plane, the kinematic viscosity and the Reynolds number were 6.4°, 6.3×10^{-6} m^2/s and 29. Alekseenko (19) experimentally observed the double-peaked waves on a film or aqueous solution of glycerin falling down a vertical tube at Re = 8. He measured time variation of thickness of periodically forced

waves at a spot on the tube surface, which showed that transition from tear-drop waves with a single capillary ripple to the double-peaked waves and vice versa occur at the observation spot when the forcing frequency is between the frequencies for the nearly sinusoidal waves and for the solitary humps.

Demekhim, Tokarev and Shkadov (1987) solved the integral boundary-layer equation with the periodic boundary conditions, and their solutions predicted stationary double-peak wave profiles at Re = 8 when the wave number was between the wave numbers for the nearly sinusoidal waves and for the solitary humps. The solution of the integral boundary-layer equation by Ramaswamy, Chippada and Joo (1996) showed that there exsist two wave profiles, i.e. a double-peaked wave profile and a closely packed tear-drop wave profile. Chang, Demekhim and Kopelevich (1992) numerically solved the boundary-layer equation without the assumption of a self-similar parabolic velocity profile in the film, and found two wave families, i.e. the first family has lower velocities than the linear velocities, and the second family has larger velocities. The profiles of waves in the first family of $\alpha \sim \alpha_o/2$ resemble the double-peaked wave profile.

Ramaswamy, Chippada and Joo (1996) numerically solved the complete Navier-Stokes equations with the periodic boundary conditions for a film falling down a vertical plane, and found that after the initial rapid growth, waves change with time periodically between a closely packed tear-drop wave profile of the maximum energy and a double-peaked wave profile of the minimum energy. They also performed direct numerical simulations for a film falling down a slightly inclined plane imposing periodic disturbances on the film flow at the entrance, and found that the simulated profiles of evolving and saturated waves at various forcing frequencies are in good agreement with the experimental observations by Liu and Gollub (1994). Their

simulations also show that the transition from single-peaked waves near the film inlet via double-peaked waves to tear-drop waves with a single capillary ripple occurs on the film falling down a slightly inclined plane at the same inclination angle, Re and forcing frequency as the experiment of Liu and Gollub (1994). The present work experimentally and theoretically revealed that the almost same transition phenomena also occurs on water films of smaller viscosity and larger surface tension, falling down a vertical plane at Reynolds numbers as large as Re ~ 50, and that the excited waves decelerate as they grow into the double-peaked waves, and then they rapidly accelerate when they grow into the nearly steady tear-drop waves with a single ripple.

References

Alekseenko, S.V., Nakoryakov, V.E. and Pokusaev, B.G. (1985) Wave formation on a vertical falling liquid film, *AIChE J.* **31**, 1446-1460.

Anshus B.E. and Goren S.L. (1966) A method of getting approximate solutions to the Orr-Sommerfeld equation for flow on a vertical wall, *AIChE J.* **12**, 1004-1008.

Bach, P. and Villadsen, J. (1984) Simulation of the vertical flow of a thin, wavy film using a finite element method, *Intl J. Heat Mass Transfer* **27**, 815-827.

Benjamin, T.B. (1957) Wave formation in laminar flow down an inclined plane, *J. Fluid Mech.* **2**, 554-574.

Benney, D.J. (1966) Long waves on liquid films, *J. Math. Phys.* **45**, 150-155.

Brauner, N. and Maron, D.M. (1982) Characteristics of inclined thin films. Waviness and the associated mass transfer, *Intl J. Heat Mass Transfer* **25**, 99-110.

Chang, H.C. (1987) Evolution of nonlinear waves on vertically falling film – A normal form analysis, *Chem. Eng. Sci.* **42**, 515.

Chang, H.C. (1989) Onset of nonlinear waves on falling film, *Phys Fluids* **A1**, 1314.

Chang, H.C. (1994) Wave evolution on a falling film, *Ann. Rev. Fluid Mech.* **26**, 103-136.

Chang, H.C., Cheng, M., Demekhin, E.A. and Kopelevich, D.I. (1994) Secondary and tertiary excitation of three-dimensional patterns on a falling film, *J. Fluid Mech.* **270**, 251.

Chang, H.C., Demekhin, E.A. and Kalaidin, E. (1995a) Interaction dynamics of solitary waves on a falling film, *J. Fluid Mech.* **294**, 123.

Chang, H.C., Demekhin, E.A. and Kopelevich, D.I. (1993) Nonlinear evolution of waves on a vertically falling film, *J. Fluid Mech.* **250**, 433-480.

Cheng, M. and Chang, H.C. (1992) Stability of axisymmetric waves on liquid films flowing down a vertical column to azimuthal and streamwise disturbances, *Chem. Eng. Commun.,* **118**, 327.

Cheng, M. and Chang, H.C. (1995) Competition between subharmonic and sideband secondary instabilities on a falling film, *Phys. Fluids* 7, 34-54.

Chin, R.W., Abernathy, F.F. and Bertschy, J.R. (1986) Gravity and shear wave stability of free surface flows. Part 1. Numerical calculations, *J. Fluid Mech.* **168**, 501-513.

Dressler, R.F. (1949) Mathematical solution of the problem of roll-waves in inclined open channels, *Commun. Pure Appl. Maths* **2**, 149-194.

Gjevik, B. (1970) Occurrence of finite-amplitude surface waves on a falling liquid films, *Phys. Fluids* **13**, 1918-1925.

Ho, L.W. and Patera, A.T. (1990) A legendre spectral element method for simulation of unsteady incompressible viscous free-surface flows, *Comput. Meth. Appl. Mech. Engng* **80**, 355-366.

Hooper, A.P. and Grimshaw, R. (1985) Nonlinear instability at the interface between two viscous fluids, *Phys. Fluids* **28**, 37-45.

Huerre, P. and Monkewitz, P.A. (1990) Local and global instabilities in spatially developing flows, *Ann. Rev. Fluid Mech.* **22**, 473.

Joo, S.W. and Davis, S.H. (1991) On falling-film instabilities and wave breaking, *Phys. Fluids* A **3**, 231-232.

Joo, S.W. and Davis, S.H. (1992) Instabilities of three-dimensional on viscous falling films, *J. Fluid Mech.* **242**, 529.

Joo, S.W. and Davis, S.H. (1992) Irregular waves on viscous falling films, *Chem. Engng Commun.* **118**, 111-123.

Joo, S.W., Davis, S.H. and Bankoff, S.G. (1991) Long-wave instabilities of heated falling films: two-dimensional theory of uniform layers, *J. Fluid Mech.* **230**, 117-146.

Kapitza, P.L. (1948) Wave flow of a thin viscous fluid layers, *Zh. Eksp. Teor. Fiz.* **18**, 1.

Kapitza, P.L. and Kapitza, S.P. (1949) Wave flow of thin layers of a viscous fluid: III. Experimental study of undulatory flow conditions, *Zh. Exp. Teor. Fiz.* **19**, 105. Also in *Collected Papers of P.L. Kapitza* (ed. D. Ter Haar), Vol 2, PP. 690-709, Pergamon (1965).

Kheshgi, H.S. and Scriven, L.E. (1987) Distrubed film flow on a vertical plate, *Phys. Fluids* **30**, 990-997.

Krantz, W.B. and Goren, S.L. (1971) Stability of thin liquid films flowing down a plane, *Indust. Engng Chem. Fundam.* **10**, 91-101.

Lin, S.P. (1969) Finite amplitude stability of a parallel flow with a free surface, *J. Fluid Mech.* **36**, 113-126.

Lin, S.P. (1983) Film waves in waves on fluid interfaces, R.E. Meyer, ed., Academic Press, p. 261.

Liu, J. and Gollub, J.P. (1993) Onset of spatially chaotic waves on flowing films, *Phys. Rev. Lett.* **70**, 2289-2292.

Liu, J. and Gollub, J.P. (1994) Solitary wave dynamics of film flows, *Phys. Fluid* **6**, 1702-1712.

Liu, J., Paul, J.D. and Gollub, J.P. (1993) Measurements of the primary instabilities of film flows, *J. Fluid Mech.* **250**, 69-101.

Liu, J., Schneider, J.B. and Gollub, J.P. (1995) Three dimensional instabilities of film flows, *Phys. Fluid* **7**, 55-67.

Nakaya, C. (1975) Long waves on a thin fluid layer flowing down an inclined Plane, *Phys. Fluid* **18**, 1407-1412.

Nakaya, C. (1989) Waves on a viscous fluid film down a vertical wall, *Phys. Fluid* **A1**, 1143.

Nosoko, T., Yoshimura, P.N., Nagata, T. and Oyakawa, K. (1996) Characteristics of two-dimensional waves on a falling liquid films, *Chem. Eng. Sci.* **51**, No. 5, 725-732.

Ooshida T. (1999) Surface equation of falling film flows with moderate Reynolds number and large but finite Weber number, *Physics of Fluids* **11**, No. 11, pp. - .

Pierson F. W. and Whitaker S. (1977) Some theoretical and experimental observations of the wave structure of falling liquid film, *Indust. Eng. Chem., Fundam.* **16**, 401-408.

Potalski, S. and Clegg, A.J. (1972) An experimental study of wave inception on falling liquid films, *Chem. Eng. Sci.* **27**, 1257-1265.

Prokopiou, TH., Cheng, M. and Chang, H.C. (1991) Long waves on inclined films at high Reynolds number, *J. Fluid Mech.* **222**, 665-691.

Pumir, A., Manneville, P. and Pomeau, Y. (1983) On solitary waves running down an

inclined plane, *J. Fluid Mech.* **135**, 27-50.

Ramaswamy, B., Chippada, S. and Joo, S.W. (1996) A full-scale numerical study of interfacial instabilities in thin-film flows, *J. Fluid Mech.* **325**, 163-194.

Roskes, G.J. (1970) Three-dimensional long waves on a liquid film, *Phys. Fluids* **13**, 1440-1445.

Salamon, T.R., Armstrong, R.C. and Brown, R.A. (1994) Traveling waves on vertical films: Numerical analysis using the finite element method, *Phys. Fluids* **6**, 2202-2220.

Shkadov, V.Ya. (1967) Wave conditions in the flow of thin layer of a viscous liquid under the action of gravity, *Izv. Akad. Nauk. SSSR Mekh. Zhidk i Gaza*, **1**, 43.

Sivashinsky, G.I. and Michelson, D.M. (1980) On the irregular wavy flow of liquid film down a vertical plane, *Prog. Theor. Phys.* **63**,2112.

Stainthorp, F.P. and Allen, J.M. (1965) The development of ripples on the surface of a liquid film flowing inside a vertical tube, *Trans. Inst. Chem. Eng*, **43**, T85-T91.

Tsvelodub, O. Yu. (1980) Steady traveling waves on a vertical film of fluid, *Izv. Akad. Nauk. SSSR Mekh. Zhidk i Gaza*, **4**, 142.

Wasden, F.K. and Dukler, A.E. (1989) Insights into the hydrodynamics of free falling wavy films. *AIChE J.* **35**, 187-195.

Whitaker, S. (1964) Effect of surface active agents on stability of falling liquid films, *Indust. Engng Chem., Fundam.* **3**, 132-142.

Yih, C.S. (1963) Stability of liquid flowing down an inclined plane, *Phys. Fluids* **6**, 34.

Table 1 Comparison between approximate solutions and direct numerical solutions to the Orr-Sommerfeld equations.

Re	α_m	c_m	α_c
10/3	0.050	2.96	0.0734
	0.054	2.96	0.0801
20/3	0.078	2.79	0.127
	0.083	2.79	0.139
100/3	0.123	2.00	0.416
	0.124	2.01	0.414
200/3	0.144	1.80	0.598
	0.140	1.80	0.606

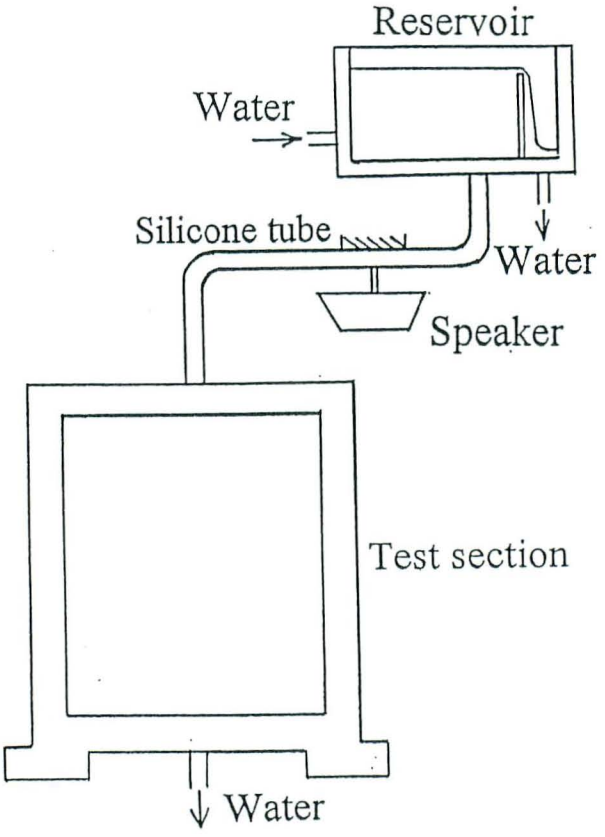
Reservoir
Water
Silicone tube
Water
Speaker
Test section
Water

Fig. 1

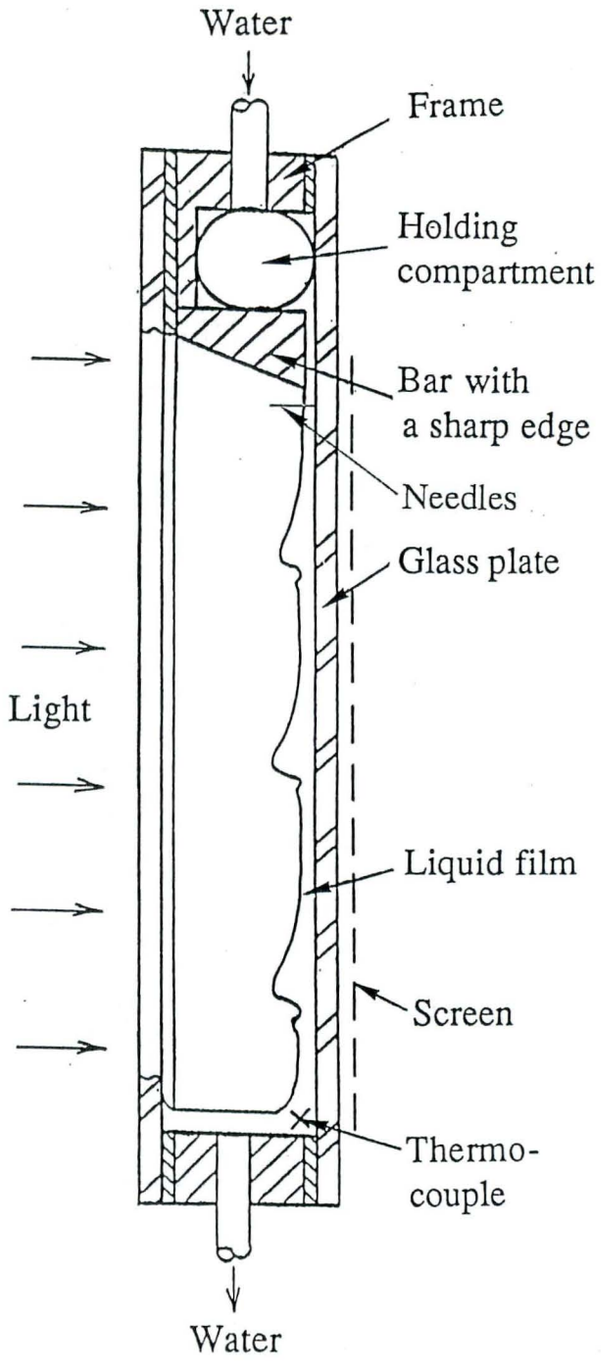
Water
Frame
Holding compartment
Bar with a sharp edge
Needles
Glass plate
Light
Liquid film
Screen
Thermo-couple
Water

Fig. 2

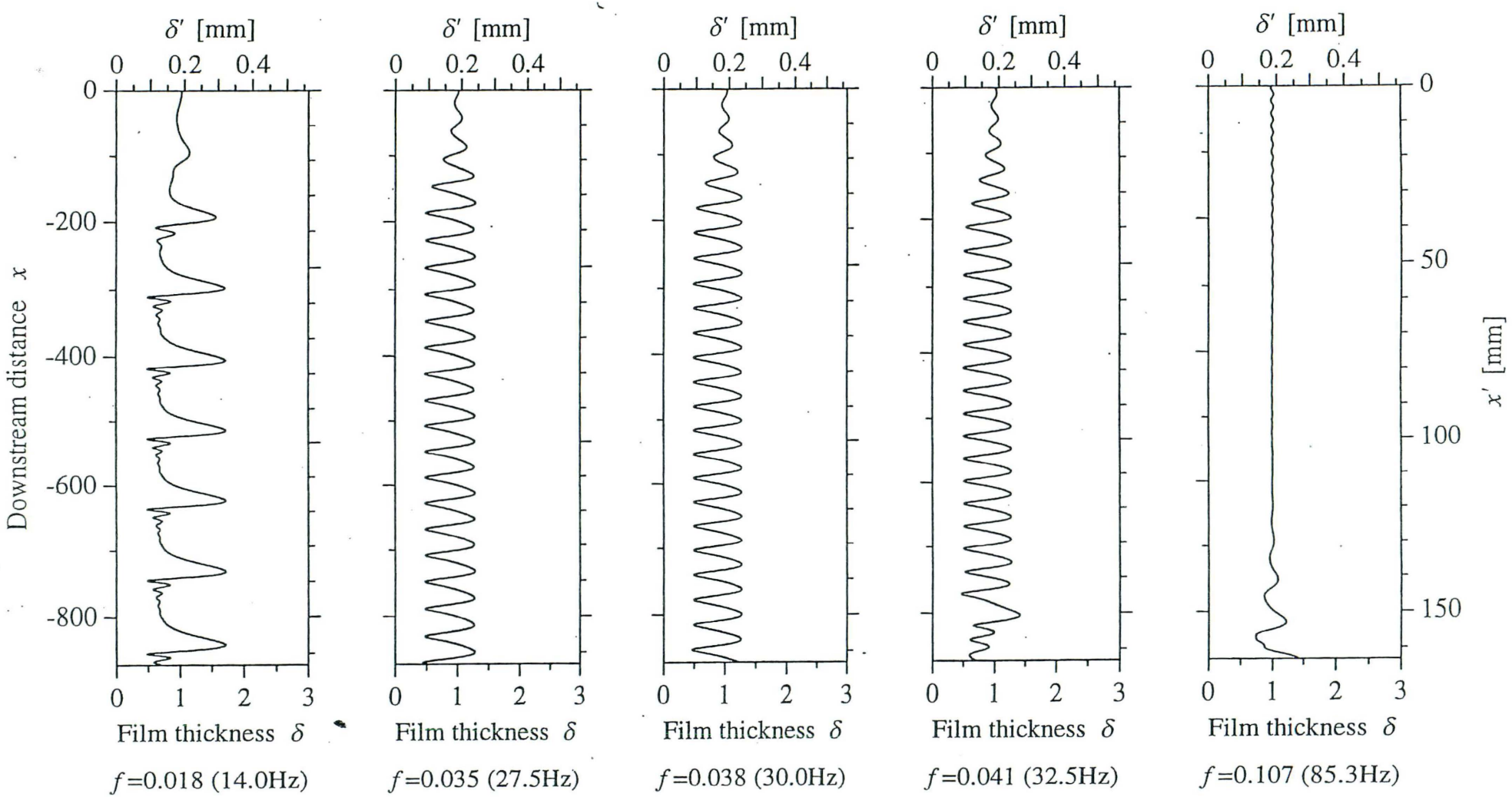
δ′ [mm]
0 0.2 0.4
0
-200
-400
-600
-800
Downstream distance x
0 1 2 3
Film thickness δ
f=0.018 (14.0Hz)
f=0.035 (27.5Hz)
f=0.038 (30.0Hz)
f=0.041 (32.5Hz)
f=0.107 (85.3Hz)
0
50
100
150
x′ [mm]

Fig. 3 Re = 16.1

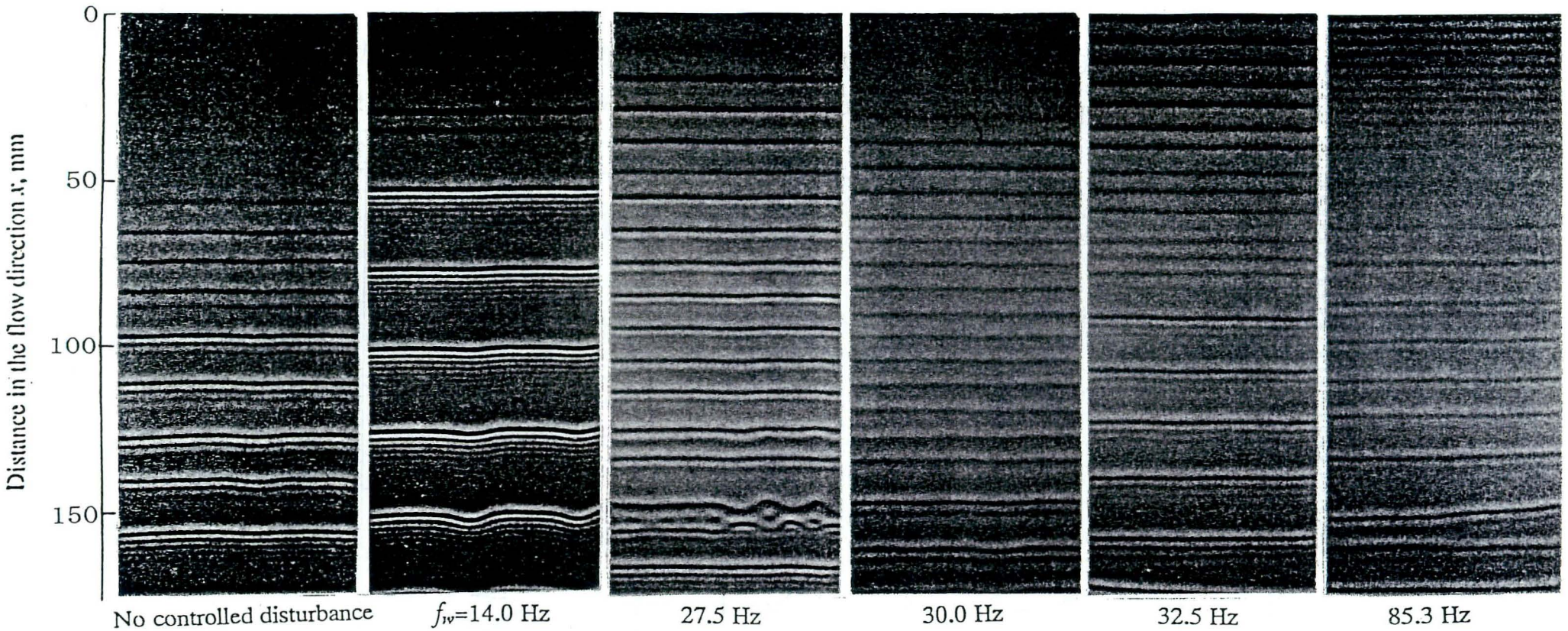
Distance in the flow direction x, mm
0
50
100
150
No controlled disturbance
f_{tv}=14.0 Hz
27.5 Hz
30.0 Hz
32.5 Hz
85.3 Hz

Fig. 4 $R_e = 16.1$

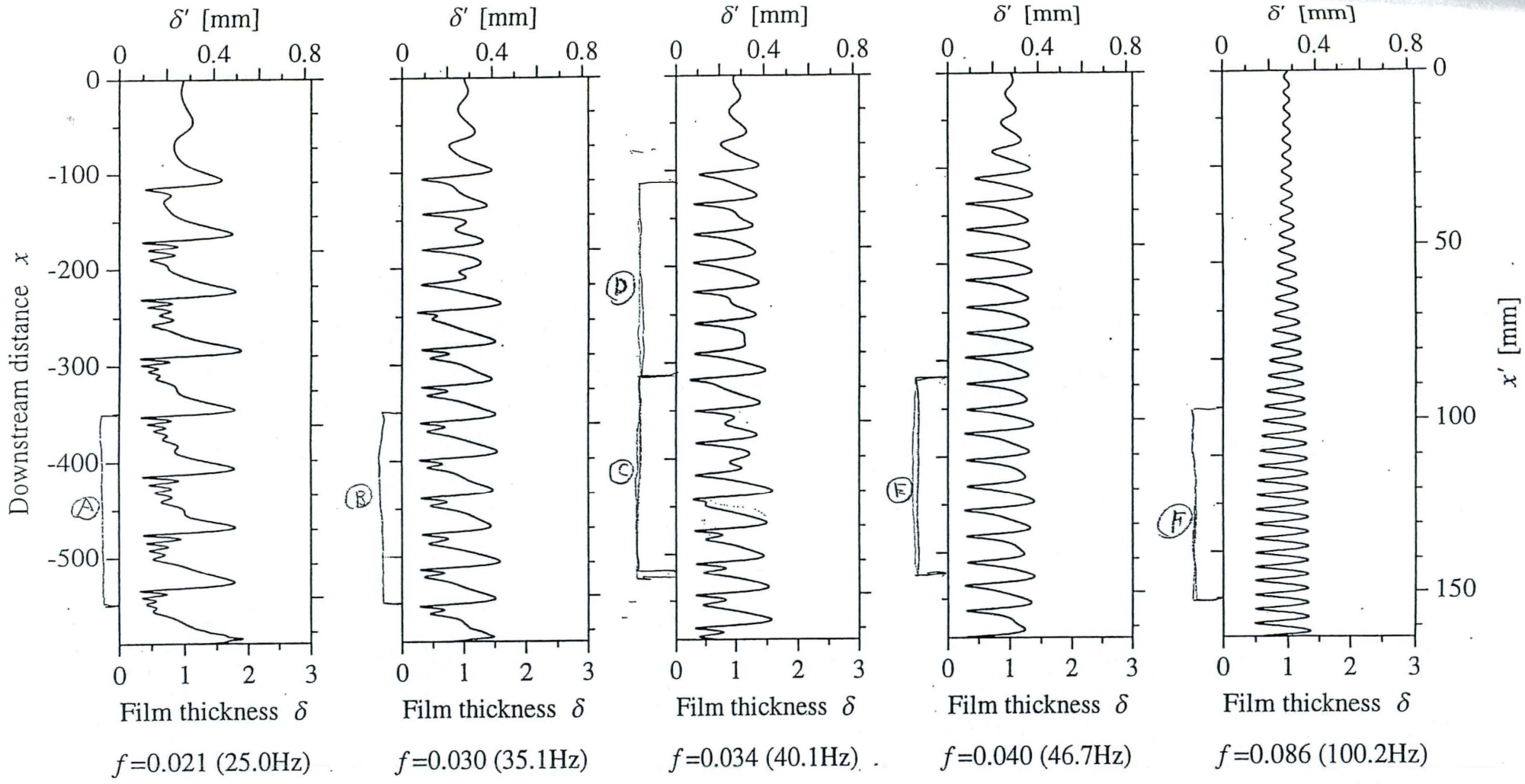
δ′ [mm]
0
0.4
0.8
Downstream distance x
0
-100
-200
-300
-400
-500
x′ [mm]
50
100
150
A
B
C
D
E
F
0
1
2
3
Film thickness δ
f=0.021 (25.0Hz)
f=0.030 (35.1Hz)
f=0.034 (40.1Hz)
f=0.040 (46.7Hz)
f=0.086 (100.2Hz)

Fig. 5 Re=51.5

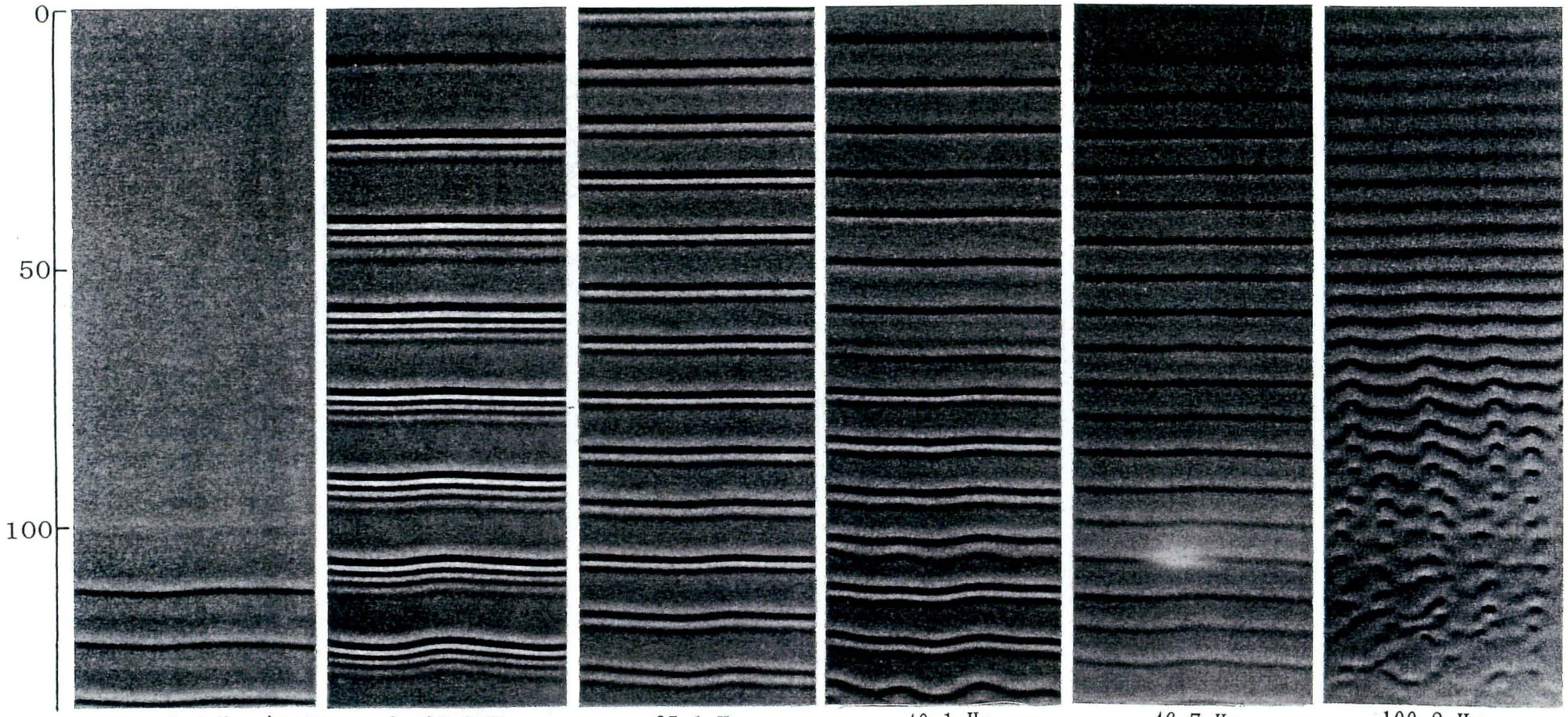
Distance in the flow direction x, mm
0
50
100
No controlled disturbance
f_w=25.0 Hz
35.1 Hz
40.1 Hz
46.7 Hz
100.2 Hz
Re=51.5

Fig. 6

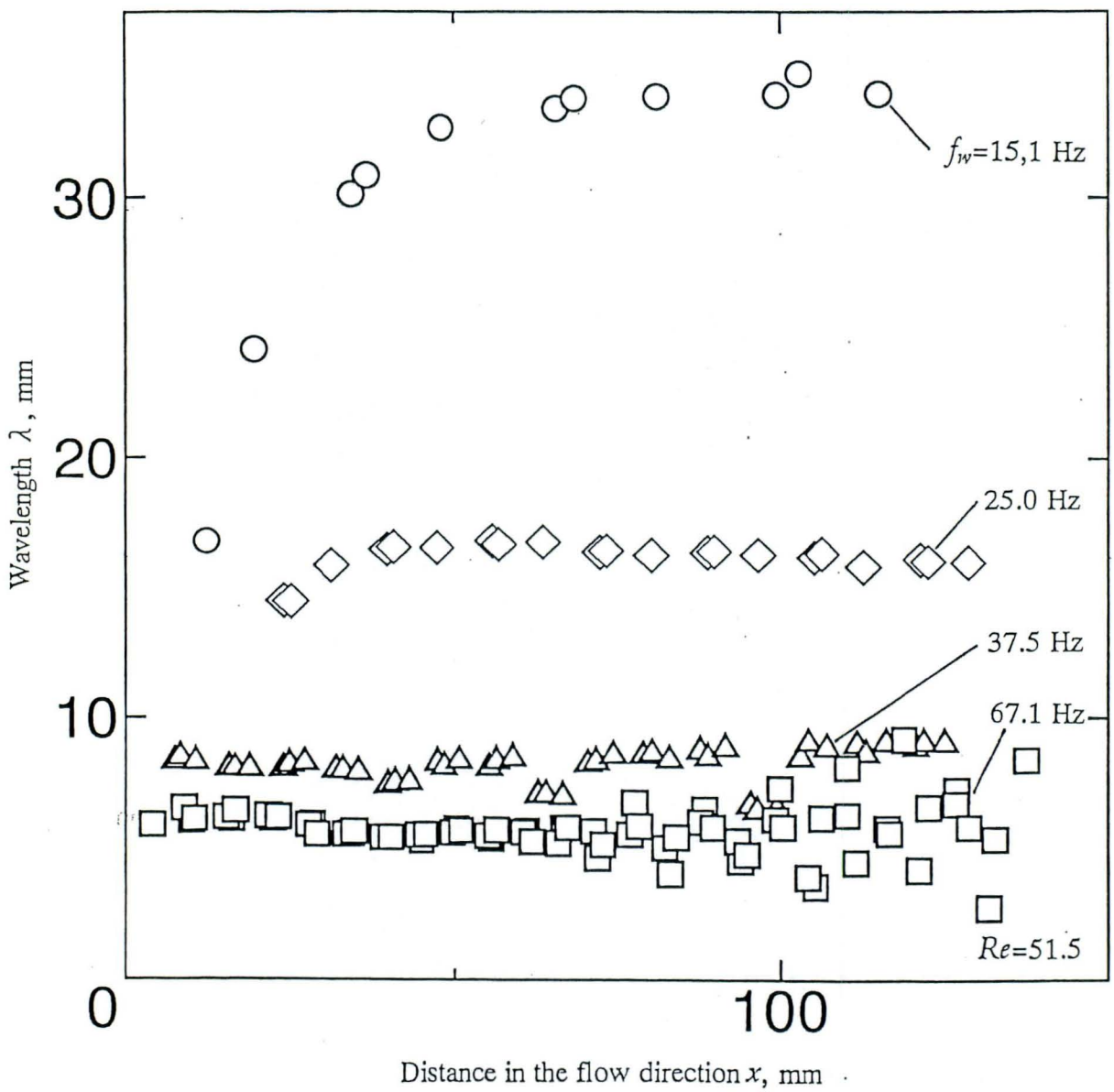
30
20
10
0
100
Wavelength λ, mm
Distance in the flow direction x, mm
f_w=15,1 Hz
25.0 Hz
37.5 Hz
67.1 Hz
Re=51.5

Fig. 7(a) Re = 51.5

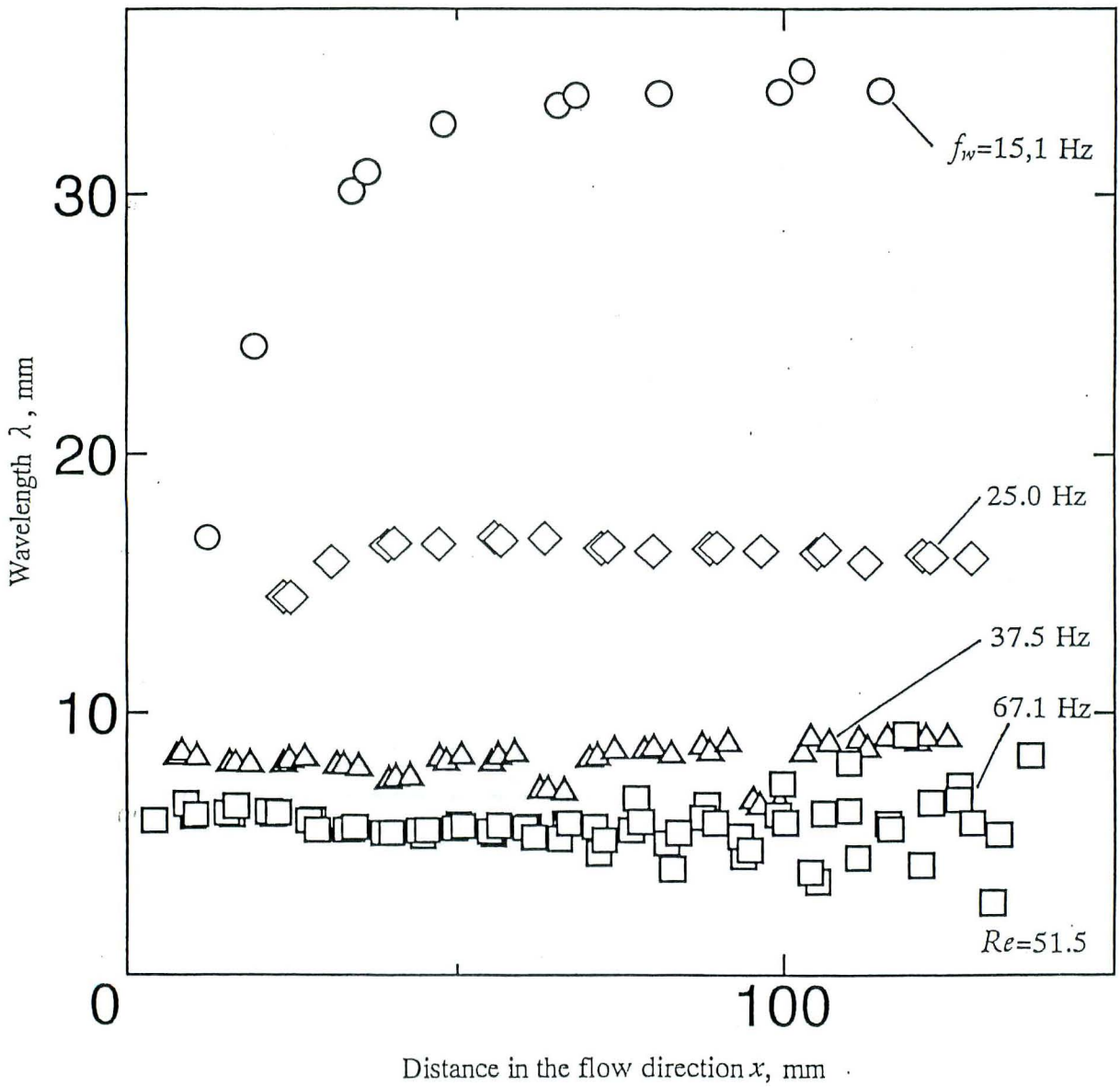
f_w=15,1 Hz
25.0 Hz
37.5 Hz
67.1 Hz
Re=51.5
30
20
10
0
100
Wavelength λ, mm
Distance in the flow direction x, mm

Fig. 7(b) $Re = 51.5$

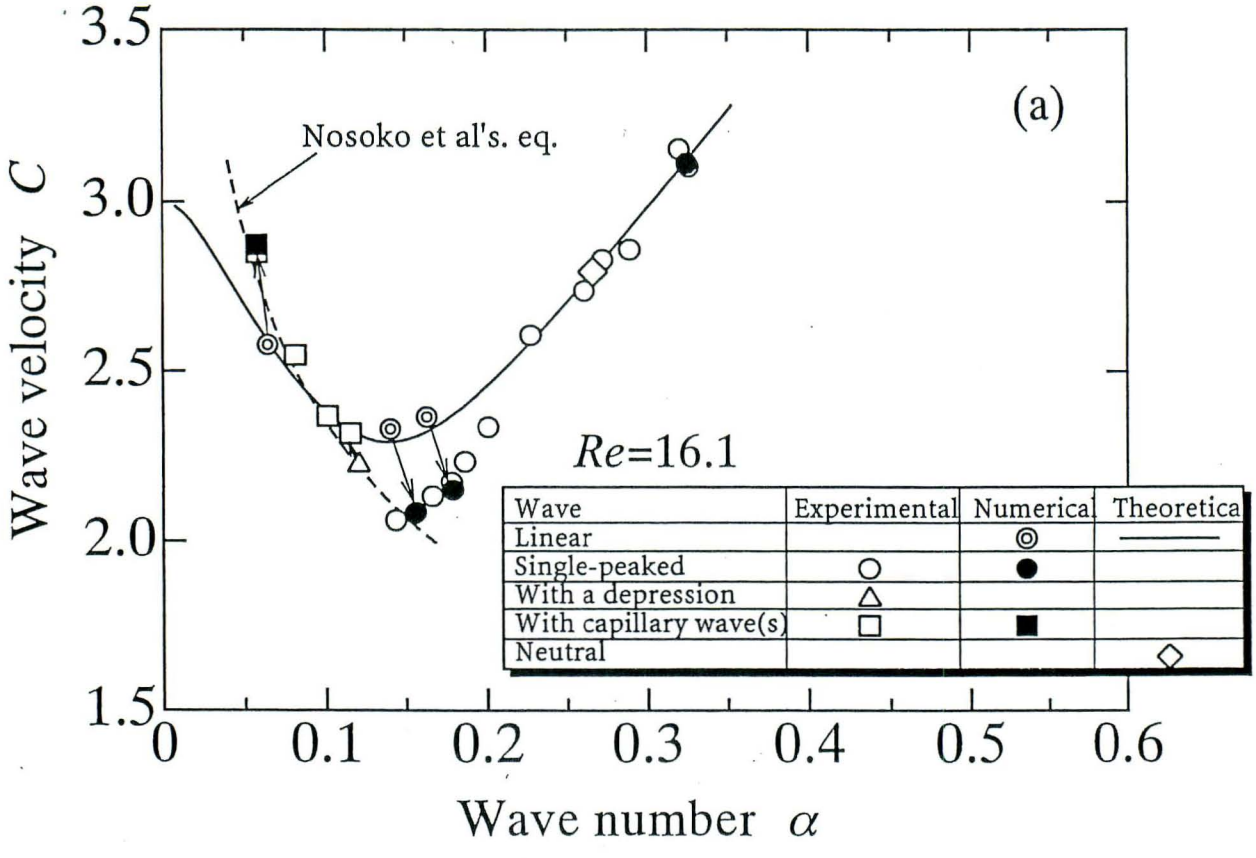
(a)
Nosoko et al's. eq.
Re=16.1
Wave velocity C
Wave number α
3.5
3.0
2.5
2.0
1.5
0
0.1
0.2
0.3
0.4
0.5
0.6
Wave | Experimental | Numerical | Theoretica
Linear
Single-peaked
With a depression
With capillary wave(s)
Neutral

Fig. 8 (a)

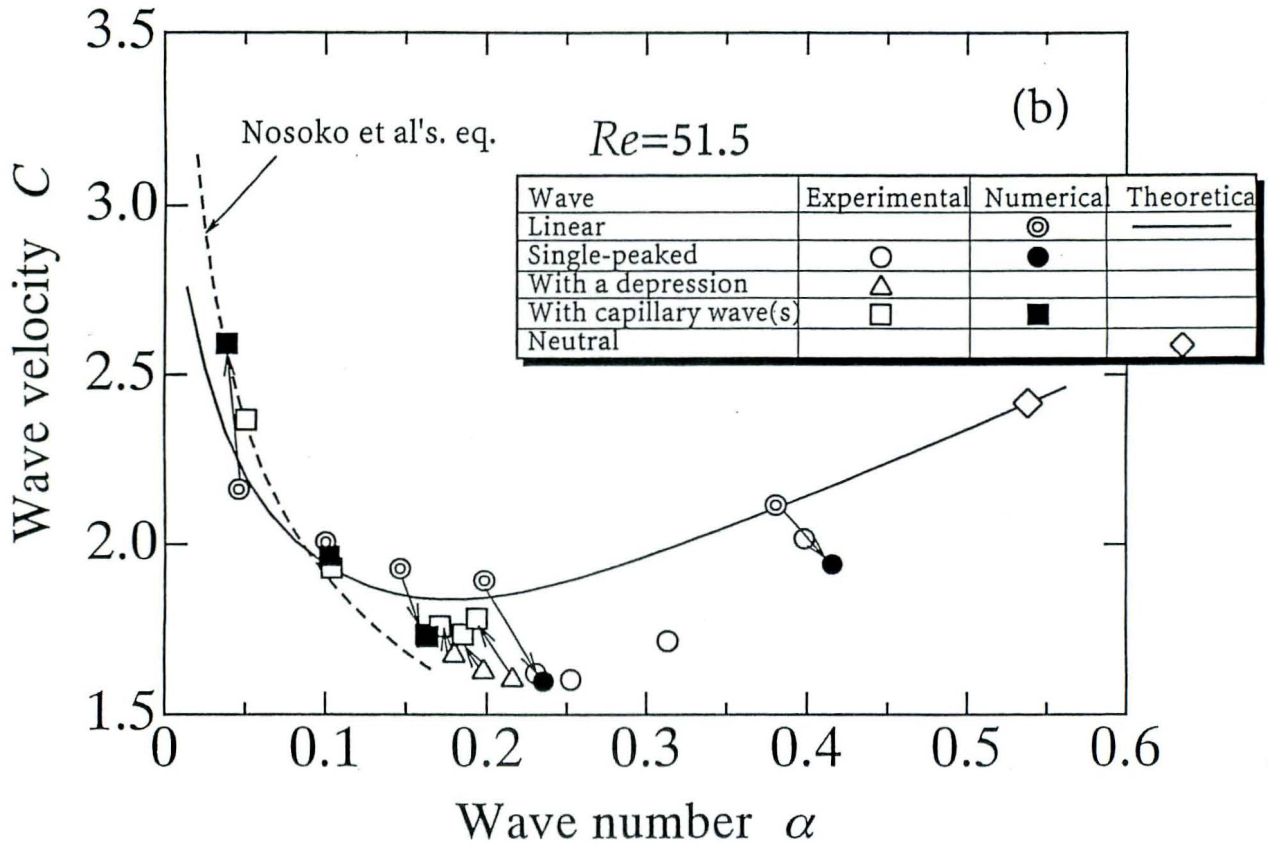
(b)
Re=51.5
Nosoko et al's. eq.
Wave
Experimental
Numerical
Theoretical
Linear
Single-peaked
With a depression
With capillary wave(s)
Neutral
Wave velocity C
Wave number α
3.5
3.0
2.5
2.0
1.5
0
0.1
0.2
0.3
0.4
0.5
0.6

Fig. 8 (b)

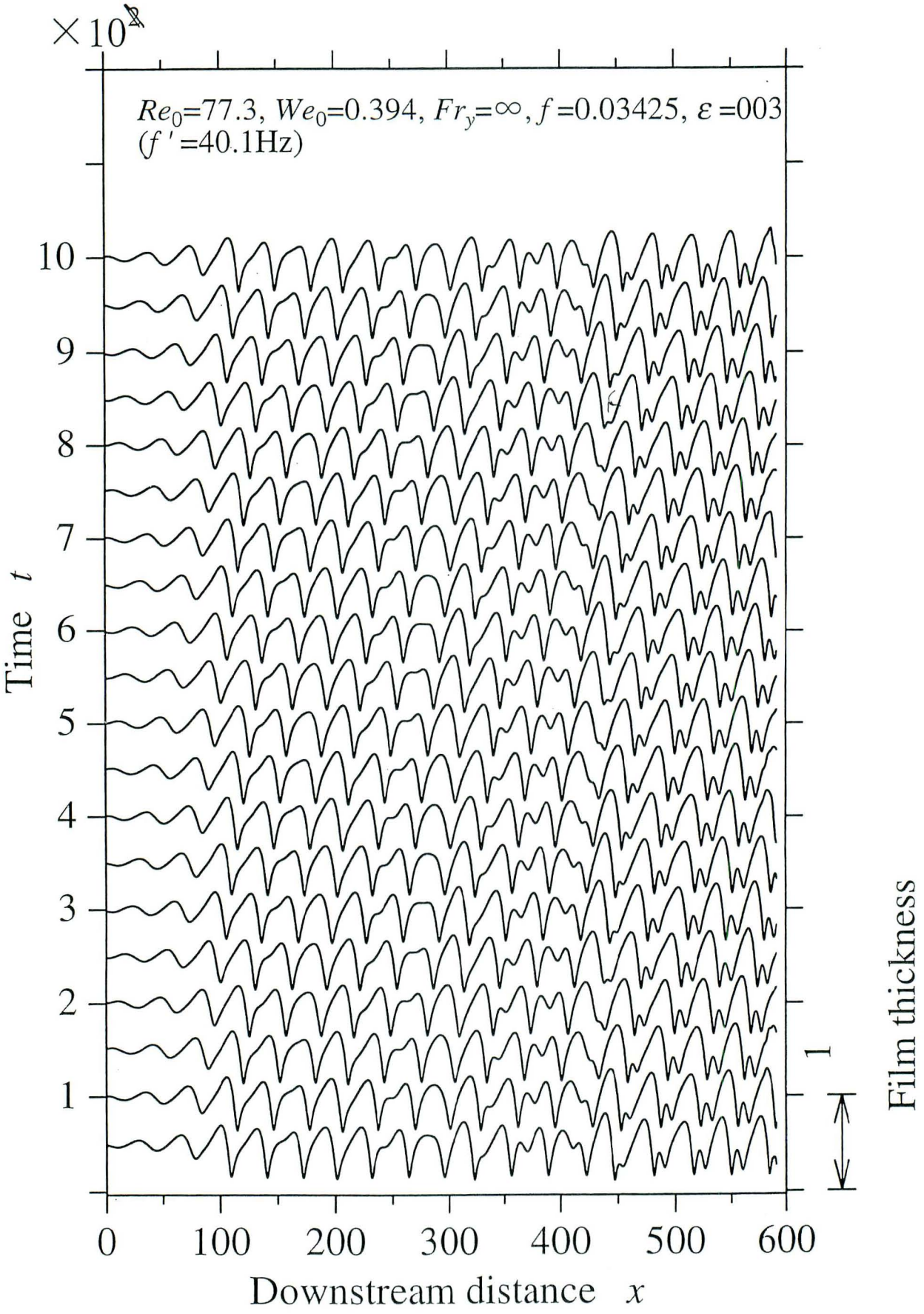
×10⁴
Re_0=77.3, We_0=0.394, Fr_y=∞, f=0.03425, ε=003
(f'=40.1Hz)
10
9
8
7
6
5
4
3
2
1
Time t
0
100
200
300
400
500
600
Downstream distance x
1
Film thickness

Fig. 9 $Re = 51.5$